International Journal of Computational Methods
Vol. 9, No. 1 (2012) 1240009 (10 pages)

DOI: 10.1142/S0219876212400099

World Scientific
www.worldscientific.com

THE BOUNDARY FACE METHOD WITH VARIABLE APPROXIMATION BY B-SPLINE BASIS FUNCTION

JINLIANG GU, ZHANG JIANMING* and XIAOMIN SHENG

State Key Laboratory of Advanced Design and Manufacturing for Vehicle Body
Hunan University, Changsha, China
**zhangjianm@gmail.com*

Received 31 December 2010
Accepted 2 June 2011

B-spline basis functions as a new approximation method is introduced in the boundary face method (BFM) to obtain numerical solutions of 3D potential problems. In the BFM, both boundary integration and variable approximation are performed in the parametric spaces of the boundary surfaces, therefore, keeps the exact geometric information of a body in which the problem is defined. In this paper, local bivariate B-spline functions are proposed to alleviate the influence of B-spline tensor product that will deteriorate the exactness of numerical results. Numerical tests show that the new method has well performance in both exactness and convergence.

Keywords: B-spline basis functions; NURBS; boundary face method; BIE.

1. Introduction

The boundary face method (BFM) has been proposed by Zhang *et al.* [2009] and implemented with approximation functions constructed by the moving least-squares (MLS) approximation. It is a generalization of the conventional boundary element method (BEM) with the development of exact geometry used for analysis. It thoroughly overcomes the shortcoming that geometric shape is crudely approximated in most FEM analyses. This paper presents a new implementation of BFM, i.e., the B-spline basis functions [Carl de Boor (1972); Lyle Ramshaw (1989)] instead of the MLS are used for approximating the boundary variables. The work is largely stimulated by the conception of isogeometric analysis [Hughes *et al.* (2005)].

The conception of isogeometric analysis is first proposed by Hughes and his collaborators to overcome some difficulties that occur in classical design loop [Hughes *et al.* (2005); Cottrell *et al.* (2007); Bazilevs *et al.* (2006); Wall *et al.* (2008)]. Its primary goal is using an exact geometric representation for analysis. Within the concept, B-spline basis functions generated from nonuniform rational B-spline

*Corresponding author.

(NURBS) play a key role in offering exact geometry representation, simplification of design optimization, and tighter integration of analysis and CAD.

Considering the important influence of B-spline basis functions, we introduce them into the framework of the BFM. Coupling the BFM with the B-spline basis functions, two distinct differences are involved comparing with traditional BEM. One is that the integrand quantities, such as the coordinates of Gauss integration points, Jacobian, and out normal are calculated directly from exact geometry instead of element approximation, an important property inherited from BFM. Another is that B-spline approximation represents continuity between elements, a distinct property that must be explicitly expressed in the BEA cases. Furthermore, a richer set of refinement operations for the basis functions makes B-spline more flexibly to be used for adaptive analysis in BFM.

In our scheme, B-spline basis functions described by the traditional global forms are converted into the local forms. Thus, construction of B-spline approximation functions will be no longer fully restricted by the fashion of tensor product, which require control points must lie topologically in a rectangular grid. This strategy largely reduces the load for computation and saves a lot of computational resource.

This paper is organized as follows. In Sec. 2, the description of local bivariate B-spline function is given here. In Sec. 3, bivariate B-spline functions as an approximate tool are used in the discretization of BIEs. Numerical examples for 3D potential problems are given in Sec. 4. Finally, we present the conclusions for our work in Sec. 5.

2. Local Bivariate B-Spline Function

Local B-spline functions are built from B-spline basis functions. The B-spline basis functions in global form are defined recursively for zero degree,

$$B_{i,k}(\xi) = \begin{cases} 1, & \xi_i \le \xi \le \xi_{i+1} \\ 0, & \text{otherwise} \end{cases} \quad k = 0, \tag{1}$$

and for nonzero degrees,

$$B_{i,k}(\xi) = \frac{\xi - \xi_i}{\xi_{i+k} - \xi_i} B_{i,k-1}(\xi) + \frac{\xi_{i+k+1} - \xi}{\xi_{i+k+1} - \xi_{i+1}} B_{i+1,k-1}(\xi), \quad k > 0. \tag{2}$$

Assuming that $0/0 := 0$ and $\Xi = [\xi_1, \xi_2, \ldots, \xi_{n+k+1}]$, where Ξ is a knot vector; ξ_i the ith knot and n the total number of basis functions corresponding to the number of control points. Knot values presented in the knot vector Ξ are given by: $\xi_1 = \xi_2 = \cdots = \xi_{k+1} = 0$, $\xi_{n+1} = \xi_{n+2} = \cdots = \xi_{n+k+1} = 1$, and $\xi_i = i/(n-k)$ for $i = k+1, k+2, \ldots n$.

Then, the local form of bivariate B-spline function can be constructed by the basis functions. It is shown as:

$$P(\xi,\eta)=\sum_{r=0}^{k}\sum_{s=0}^{l}N_{rs}(\xi,\eta)p_{rs}, \tag{3}$$

where $N_{rs}(\xi,\eta)$ is defined by:

$$N_{rs}(\xi,\eta)=\begin{cases}B_{i-r,k}^{(r+1)}(\xi)B_{j-s,l}^{(s+1)}(\eta), & \xi\in[\xi_i,\xi_{i+1}),\quad \eta\in[\eta_j,\eta_{j+1})\\ 0, & \text{otherwise}\end{cases}, \tag{4}$$

$p_{ij}(p_{x_{ij}},p_{y_{ij}},p_{z_{ij}})$ are a set of control points. ξ and η are parametric coordinates with their values lying in the $[\xi_1,\xi_2,\ldots,\xi_{n+k+1}]$ and $[\eta_1,\eta_2,\ldots,\eta_{m+l+1}]$, respectively. Here, $p_{rs}=p_{(i-r)(j-s)}$, $[\xi_i,\xi_{i+1})$ and $[\eta_j,\eta_{j+1})$ are nonzero intervals.

3. Discretization of the BIE for Potential Problem

3.1. *BIE for potential problem*

Given boundary conditions, the self-regular BIE corresponding to the Laplace's equation can be written as:

$$0=\int_\Gamma(u(s)-u(y))q^s(s,y)\mathrm{d}\Gamma-\int_\Gamma q(s)u^s(s,y)\mathrm{d}\Gamma, \tag{5}$$

where u and q are respectively potential and flux functions on the boundary Γ, which is approximated by local bivariate B-spline functions in our paper. S is the field point and y is the source point. $u^s(s,y)$ and $q^s(s,y)$ are the fundamental solutions. For the 3D potential problems,

$$u^s(s,y)=\frac{1}{4\pi r(s,y)}, \tag{6}$$

$$q^s(s,y)=\frac{\partial u^s(s,y)}{\partial n(s)}=\frac{1}{4\pi r^2(s,y)}\cdot\sum_{i=1}^{3}\frac{x_i(s)-x_i(y)}{r(s,y)}\cdot n_i(s), \tag{7}$$

where r is the spatial distance from source point to field point.

Substituting the Eq. (3) into Eq. (5) and discretizing the BIE, we obtain the discrete form:

$$0=\sum\int_{\Gamma_{ij}}(u(s)-u(y))q^s(s,y)\mathrm{d}\Gamma-\sum\int_{\Gamma_{ij}}q(s)u^s(s,y)\mathrm{d}\Gamma. \tag{8}$$

Assumed that $\Gamma_{ij}=\{(\xi,\eta)|\xi\in[\xi_i\xi_{i+1}),\eta\in[\eta_j\ \eta_{j+1})\}$ and given the following substitutions:

$$I_{ij}^{(1)}=\int_{\Gamma_{ij}}(u(s)-u(y))q^s(s,y)\mathrm{d}\Gamma,\quad I_{ij}^{(2)}=\int_{\Gamma_{ij}}q(s)u^s(s,y)\mathrm{d}\Gamma, \tag{9}$$

which can be further written as:

$$I_{ij}^{(1)} = \sum_{r=0}^{k}\sum_{s=0}^{l}\left(\int_{-1}^{1}\int_{-1}^{1}\left(\tilde{N}_{rs} - \tilde{N}_{rs}(\xi_0,\eta_0)\right)q^s(\xi,\eta)J(\xi,\eta)\mathrm{d}\xi\mathrm{d}\eta\right)\tilde{u}_{rs} \tag{10}$$

$$I_{ij}^{(2)} = \sum_{r=0}^{k}\sum_{s=0}^{l}\left(\int_{-1}^{1}\int_{-1}^{1}\tilde{N}_{rs}u^s(\xi,\eta)J(\xi,\eta)\mathrm{d}\xi\mathrm{d}\eta\right)\tilde{q}_{rs}. \tag{11}$$

Then, Eq. (5) can be expressed as the matrix form:

$$\mathbf{H}\tilde{\mathbf{u}} - \mathbf{G}\tilde{\mathbf{q}} = \mathbf{0}. \tag{12}$$

4. Numerical Examples

Two 3D exact geometric models for potential problems are employed in the BFM to illustrate the efficiency and accuracy of B-spline approximation. The boundary geometric information used for solving the BIEs, such as the Jacobian, the out normal, and the distance between two points, can be exactly obtained from the exact geometry of a body based on the conception of BFM.

To estimate numerical error and convergence, a "global" L_2 norm error, normalized by $|v|_{\max}$ is defined by Zhang *et al.* [2004]:

$$e = \frac{1}{|v|_{\max}}\sqrt{\frac{1}{N}\sum_{i=1}^{N}\left(v_i^{(e)} - v_i^{(n)}\right)^2}, \tag{13}$$

where $|v|_{\max}$ is the maximum value of sample points and the superscripts (e) and (n) refer to the exact and numerical solutions, respectively.

4.1. *The potential problem*

To assess the accuracy of B-spline approximation method, we use the following three analytical fields, which are taken from the paper by Zhang *et al.* [2004].

(i) Quadratic solution:

$$u = -2x^2 + y^2 + z^2. \tag{14}$$

(ii) Cubic solution:

$$u = x^3 + y^3 + z^3 - 3yx^2 - 3xz^2 - 3zy^2. \tag{15}$$

In all cases, BIEs generated from Laplace's equation $\nabla^2 u = 0$ is solved, combined with reasonable prescribed boundary conditions corresponding to the above analytical solutions.

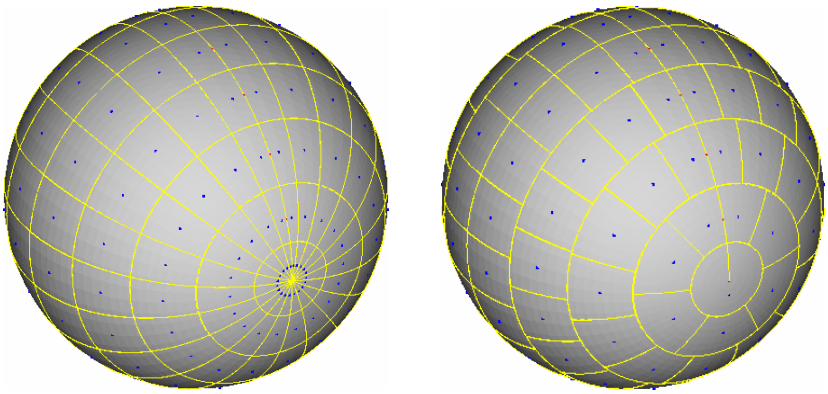

(a) (b)

Fig. 1. Two different mesh models for the sphere: (a) mesh according to global B-spline definition and (b) mesh according to local B-spline definition.

4.1.1. *Potential problem for a sphere*

A sphere is first used for discussion, with radius 2 unit and center at the origin. The usual spherical polar coordinates θ and φ are used. The Dirichlet boundary condition is employed in the discussion. Comparison among quadratic and cubic B-spline functions, as well as MLS will be carried out on the sphere. The Dirichlet boundary conditions corresponding to the exact solutions (Eqs. (14)–(15)) are imposed on the surface of the sphere. Three sets of nodes: (a) 29 nodes, (b) 118 nodes, and (c) 277 nodes are used for obtaining the numerical results. Two kinds of comparison are used for illustrating the B-spline approximation. In the first one, two fashions of meshes are adopted to testify their computational efficiency. Mesh displayed in Fig. 1(b) indicates that elements (also called nodes) are located along woofs, the number of elements can be modified according to the woofs length. Therefore, the element size in the full surface can be modified near to a uniform size.

whereas, mesh displayed in Fig. 1(a) indicates that the number of nodes along each woof keeps a fixed quantity according to B-spline basis global definition. Therefore, elements are dense in the areas of two poles of the sphere. We distribute the same number of elements (40 elements) in the two sides of equators; 200 nodes are used for subdividing the full surface in Fig. 1(a), but only 118 nodes are used in Fig. 1(b). Numerical test is performed between the two different mesh models. The L_2 errors of nodal values of q (denoted by Err_q) evaluated by Eq. (13) and time required for constructing the coefficient matrices (denoted by Mat_t) for various analytical fields are described in Table 1. The L_2 errors are signed with percentage (%). Quadratic and cubic B-spline basis functions are employed to make the comparison. From the data described in Table 1, we can clearly find much efficiency can be introduced in the example from the local definition of basis functions, not only in exactness, but also in time cost.

Table 1. The L_2 errors of q and computational time from two kinds of meshes.

Number of nodes	Analytical field	Degree of B-spline	Err_q(%)	Mat_t(s)
118 (Local B-spline)	$u =$ quadratic	two degree	**0.1609**	**117**
		three degree	**0.06234**	**271**
	$u =$ cubic	two degree	**0.4574**	**196**
		three degree	**0.1488**	**172**
200 (Global B-spline)	$u =$ quadratic	two degree	2.245	890
		three degree	2.088	860
	$u =$ cubic	two degree	2.594	805
		three degree	2.434	750

Table 2. The L_2 error of components of potential u and flux q, for Dirichlet problems on a sphere.

Number of nodes		u (D)	q_z (D)	q (S)	q_y (S)	q_z (N)	Time (s)
29	B.	5.801	18.18	5.557	22.05	6.182	6
	M.	2.036	18.48	2.58	11.37	4.915	7
58	B.	0.4816	3.851	1.392	10.38	1.15	9
	M.	0.3058	4.214	1.125	9.405	1.437	11
78	B.	0.05612	0.07807	1.467	2.664	0.5647	23
	M.	0.2186	0.9159	1.045	6.981	0.8239	28
118	B.	0.02391	0.04935	0.348	0.7733	0.1488	56
	M.	0.1791	0.3986	0.3927	4.791	0.3851	67
176	B.	0.007535	0.02501	0.108	0.3671	0.10262	117
	M.	0.04059	0.3333	0.14	2.968	0.2224	187
277	B.	0.005735	0.00267	0.02242	0.1213	0.07536	499
	M.	0.02055	0.2086	0.04361	1.367	0.1328	646

Next, comparison between MLS approximation and B-spline approximation is performed in the same framework of BFM. Numerical results in terms of components of potential u and flux q are shown in Table 2. In this case, the Dirichlet boundary condition corresponding to Eq. (14) is imposed on the surface of the sphere. According to the data from Table 2, high rates of convergence with approximation by cubic B-spline basis functions are shown in the Fig. 2. Comparing with MLS, Table 2 indicates that the B-spline basis functions maintain less time-consuming, high rates of convergence, and more accuracy.

4.1.2. *Potential problem for a convex body with a circle hole*

Here, we use a convex body for analysis, its geometry and main size are described in Fig. 3. The body is closed by three different parts of torus surfaces, two cylinder surfaces, and two discal planes. Dirichlet boundary conditions corresponding to the exact solutions (Eqs. (14)–(15)) are imposed on all of faces. There are three sets of nodes, (a) 244 nodes, (b) 452 nodes, and (c) 741 nodes, to be used for discretizing

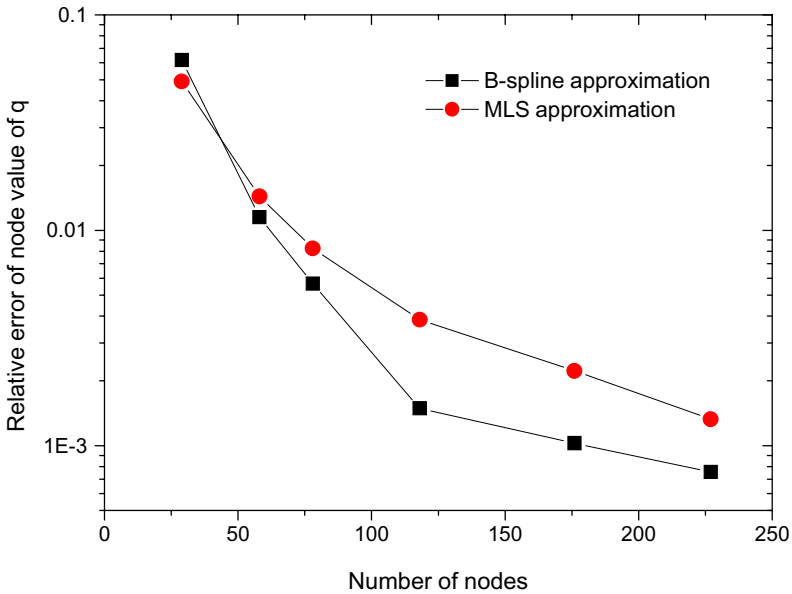

Fig. 2. Relative error and convergence of two methods.

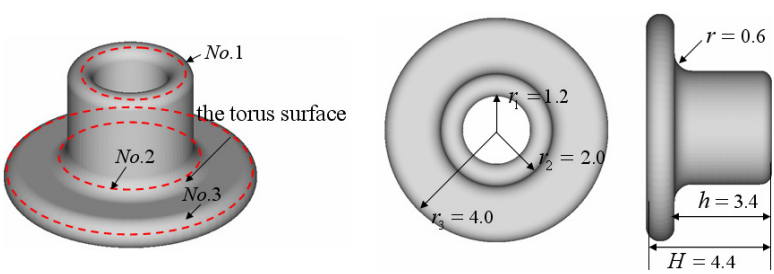

Fig. 3. A convex body with a circle hole and its main size.

this body surface. B-spline approximation functions for each face can be constructed by a free selection of degrees in two directions respectively. For example, the torus surface labeled in Fig. 3, we use cubic basis function for approximation in the circumference direction, whereas use quadratic basis function in another direction. The L_2 errors of nodal values of q (denoted by Err_q) evaluated by Eq. (14) for various analytical fields are shown in Table 3.

Table 3. Variation in L_2 error of q obtained by different sets of nodes for Dirichlet problems on a convex body.

	Number of nodes	244	452	741
u = quadratic	Err_q (%)	1.645	1.159	0.5919
u = cubic	Err_q (%)	1.878	0.5794	0.389

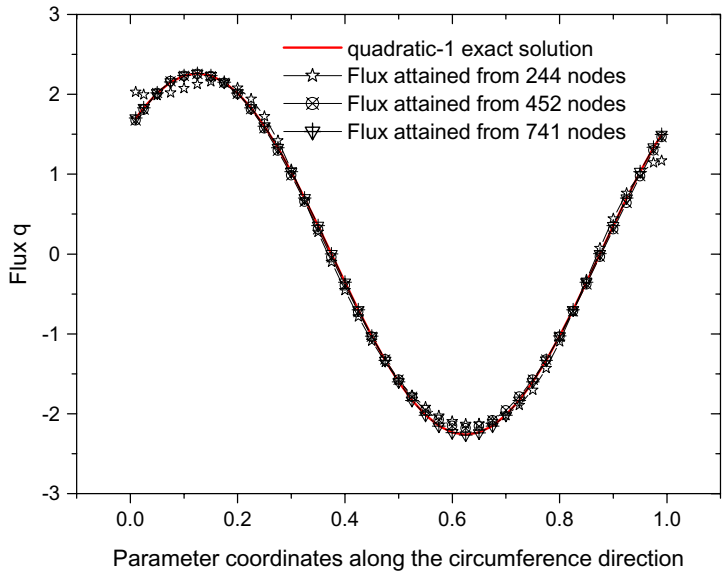

Fig. 4. Normal flux q on the No. 2 surface.

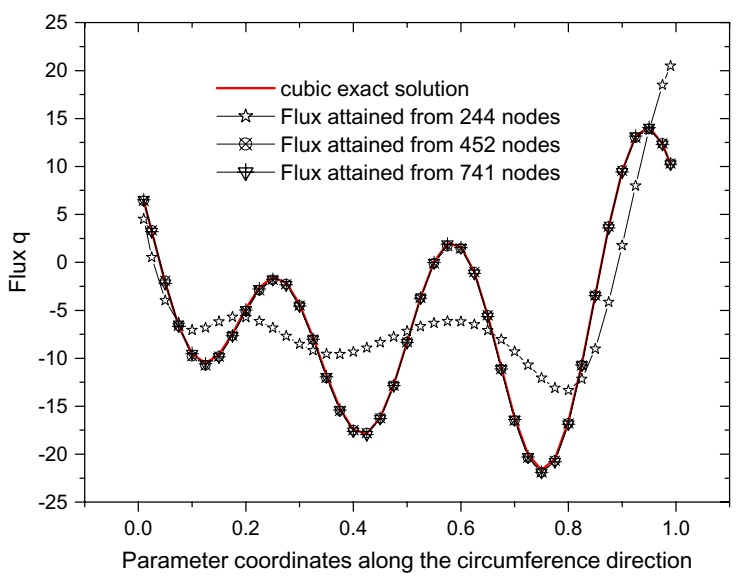

Fig. 5. Normal flux q on the No. 3 surface.

In order to determine the convergence rate, the normal flux q for three slightness surfaces labeled in the Fig. 3 are considered. In Fig. 4, the numerical results obtained with the node sets (b) and (c) are in good agreement with the quadratic-2 exact solutions. Figure 5 indicates that the numerical results also are stably convergent to

the cubic exact solution even if the results obtained from the node sets (a) fluctuate widely.

5. Conclusion

The bivariate B-spline function as an efficient approximation method has been successfully implemented in the BFM for solving the BIEs. The new implementation inherits the advantages of the BFM. For example, the geometric model of a body is directly used for analysis, thus no geometric error introduced. To alleviate the difficulties in meshing associated with the tensor product form of the B-spline bivariate functions, the traditional global form of B-spline basis functions are converted into local form. As the B-spline bivariate functions are fitting type functions, i.e., they lack the Kronecker delta property, an inverse transformation is performed to convert them into ones of interpolation type.

Numerical results have demonstrated that our implementation is feasible for solution of BIEs. As a comparison, the MLS approximation, which is widely applied in meshless analysis, is also implemented into the same framework of BFM. Comparisons between the B-spline bivariate function and the MLS approximation regarding to accuracy, stability, and efficiency have been performed using examples of potential problems. Results show that our method performs better in all mentioned aspects.

To deal with the large-scale computations for complicated geometric bodies, the fast multipole method (FMM) [Zhang *et al.* (2005); Zhang and Tanaka (2007, 2008)] can be applied to reduce the computation expense. Moreover, this is planned.

Acknowledgments

This work was supported in part by National Science Foundation of China under grant number 10972074 and in part by project under grant number 2011ZX04003-011.

References

Bazilevs, Y., de Veiga, L. B., Cottrell, J., Hughes, T. and Sangalli, G. [2006] Isogeometric analysis: approximation, stability and error estimates for refined meshes, *Math. Models Methods Appl. Sci.* **6**, 1031–1090.

Chati, M. K. and Mukherjee, S. [2000] The boundary node method for three-dimensional problems in potential theory, *Int. J. Numer. Meth. Eng.* **47**, 1523–1547.

Cottrell, J., Hughes, T. and Reali, A. [2007] Studies of refinement and continuity in isogeometric analysis, *Comput. Methods Appl. Mech. Eng.* **196**, 4160–4183.

de Boor, C. [1972] On Calculating with B-spline, *J. Approx. Theory* **6**, 50–62.

Hughes, T. J. R., Cottrell, J. A. and Bazilevs, Y. [2005] Isogeometric analysis: CAD, finite elements, NURBS, exact geometry and mesh refinement, *Comput. Meth. Appl. Mech. Eng.* **194**, 4135–4195.

Ramshaw, L. [1989] Blossoms are polar forms, *Comput. Aided Geom. Des.* **6**, 323–358.

Shaw, A. and Roy, D. [2008] NURBS-based parametric mesh-free methods, *Int. J. Numer. Meth. Eng.* **197**, 1541–1567.

Wall, W. A., Frenzel, M. A. and Cyron, C. [2008] Isogeometric structural shape optimization, *Comput. Meth. Appl. Mech. Eng.* **197**, 2976–2988.

Zhang, J. M., Tanaka, M. and Matsumoto, T. [2004] Meshless analysis of potential problems in three dimensions with the hybrid boundary node method, *Int. J. Numer. Meth. Eng.* 1147–1166.

Zhang, J. M., Tanaka, M. and Endo, M. [2005] The hybrid boundary node method accelerated by fast multipole method for 3D potential problems, *Int. J. Numer. Meth. Eng.* **63**, 660–680.

Zhang, J. M., Qin, X. Y., Han, X. and Li, G. Y. [2009] A boundary face method for potential problems in three dimensions, *Int. J. Numer. Meth. Engng.* **80**, 320–337.

Zhang, J. M. and Tanaka, M. [2007] Adaptive spatial decomposition in fast multipole method. *J. Comput. Phys.* **226**, 17–28.

Zhang, J. M. and Tanaka, M. [2008] Fast HdBNM for large-scale thermal analysis of CNT-reinforced composites, *Comput. Mech.* **41**, 777–787.

Zhang, J. M. and Yao, Z. H. [2002] Analysis of 2-D thin structures by the meshless regular hybrid boundary node method, *Acta Mech. Sin.* **15**, 36–44.